# Density of states in a two-dimensional electron gas: Impurity bands and band tails

A. Gold,* J. Serre, and A. Ghazali
*Groupe de Physique des Solides de l'Ecole Normale Supérieure, Université Paris 7, Tour 23, 2 place Jussieu, F-75251 Paris 5, France*
(Received 23 March 1987)

We calculate the density of states of a two-dimensional electron gas in the presence of charged impurities within Klauder's best multiple-scattering approach. The silicon metal-oxide-semiconductor (MOS) system with impurities at the interface is studied in detail. The finite extension of the electron wave function into the bulk is included as well as various dependences of the density of states on the electron, the depletion, and the impurity densities. The transition from an impurity band at low impurity concentration to a band tail at high impurity concentration is found to take place at a certain impurity concentration. If the screening parameter of the electron gas is decreased, the impurity band shifts to lower energy. For low impurity density we find excited impurity bands. Our theory at least qualitatively explains conductivity and infrared-absorption experiments on impurity bands in sodium-doped MOS systems and deep band tails in the gap observed for high doping levels in these systems.

## I. INTRODUCTION

The band structure and the formation of an impurity band (IB) are of vital importance for the understanding of the electronic properties of two-dimensional systems. The relevant quantity is the density of states (DOS). In this paper we calculate the DOS of a two-dimensional electron gas in the presence of disorder.

A two-dimensional electron gas can be realized in the inversion or accumulation layer of a silicon metal-oxide-semiconductor field-effect transistor (MOSFET) structure. By applying a gate voltage between the metal and the semiconductor, a two-dimensional electron gas is formed near the oxide-semiconductor interface. The electron density can be varied by means of the gate voltage. By drifting sodium ions to the interface, the formation of an IB and the transition to a band tail (BT) can be studied experimentally. The density of sodium ions can be determined in the experiment. In this sense, a sodium-doped silicon MOSFET is a well-defined model system in order to study the effects of disorder on the electronic properties of a two-dimensional electron gas. The distance between the electron gas and the oxide-semiconductor interface depends on the depletion density. Our model system is characterized by three parameters: the electron density, the impurity density, and the depletion density. For a review see Ref. 1.

Consider a two-dimensional electron gas at a low electron density. A charged impurity at the interface will bind an electron, and a Coulomb-like bound state is created. With increasing impurity concentration, a broadening of these bound states into an IB is expected. For even higher impurity concentrations, the IB will overlap with the conduction band (CB) and a BT description may be adequate. The density of states and the transport properties of the electron gas are expected to be quite different under these different circumstances.

The transport properties of the electron gas for low temperatures are determined by two scattering mechanisms. At low electron density, impurities at or near the interface determine the conductivity. For high electron density, the surface-roughness scattering becomes dominant. For a review see Ref. 1.

In the dc conductivity versus density measurements, a peak structure for an impurity density between $10^{11}$ and $10^{12}$ $cm^{-2}$ has been found in sodium-doped silicon MOSFET systems.[2,3] This peak was interpreted in terms of an IB. At higher impurity concentrations the peak structure disappeared. The conductivity at the peak was found to be strongly dependent on the temperature. This behavior indicates that the electrons are bound or localized. The dependence of the peak structure on the impurity density, the electric field at the interface, and the temperature have been measured recently.[4]

In the above-mentioned experiments,[2-4] the IB was found in conductivity measurements. The relation to the DOS seems to be clear. Direct experimental information on the DOS is obtainable from deep-level transient spectroscopy (DLTS). These experiments test the DOS in the depth of the band gap. A wide BT, depending on the impurity concentration, was found below the CB in sodium-doped silicon MOSFET systems.[5]

Most theoretical work in connection with experiments on IB's has been carried out in the limit of a single impurity. In this case, the energy spectrum of the electron in the Coulomb-like potential of the impurity has been calculated. Assuming that the electron cannot penetrate the oxide, the lowest bound state is a hydrogenlike $2p$ state with a binding energy of 0.25 Ry.[6] The finite gate voltage gives rise to an additional triangular potential which pushes the electron gas to the interface. For an ideally two-dimensional Coulomb problem, the ground state is a bound state with a binding energy of 4.0 Ry. In a real MOSFET system, the binding energy is located between these two limiting values.[7]

Binding energies for the single-impurity problem have

 

been calculated in various approximations.[8–12] It was found that the lowest bound state has an energy of about 1 Ry in the silicon MOSFET and that the electric field dependence does not play a very important role. Screening effects, however, reduce the binding energy by orders of magnitude.[12,13] It is clear that in the single-impurity approach the width of the IB cannot be calculated; in addition it is impossible to calculate the critical impurity density, where the IB begins to overlap with the CB.

IB's in silicon MOSFET systems have been treated theoretically only recently.[14] In this case the Ishida-Yonezawa method[15] was used. It is also a multiple-scattering theory based on the Matsubara-Toyozawa scheme which uses a tight-binding description for the DOS. It is essentially a single-band scheme. Therefore it cannot account for the conduction band. A BT description is therefore not possible. The reason is that there the IB is not treated as the effect of a perturbation on the CB but rather as a band in an amorphous system. Particularly in this approach, an IB will always exist, independently of $N_i$.

There exist two other calculations on the DOS for a two-dimensional electron gas. The work in Ref. 16 for quantum wells treats the strong deviations of the DOS in comparison to the ideal two-dimensional DOS near the CB. IB's are not discussed there. The deep band tail, due to impurity concentration fluctuations according to Halperin and Lax,[17] is discussed for quantum wells in Ref. 18. IB formation has not been formulated within this approach. Impurity concentration fluctuations are not considered in the present work but could be described within our theory, as it was done for three-dimensional systems in Ref. 19.

The electronic transport properties of disordered electron systems have been studied in some detail in recent years. For a review see Ref. 20. The absence of a metallic behavior at zero temperature in a noninteracting electron system for dimension $d \leq 2$ for arbitrarily weak disorder was suggested by the scaling hypothesis for the Anderson localization problem due to the existence of quantum interference effects.[21] In the scaling approach, the assumption that the DOS is finite is essential. For a noninteracting electron gas with disorder, Wegner[22] pointed out that no impurity band exists and the DOS is always finite within the band.

In the following we will show that for an interacting electron system with charged impurities, a gap in the density of states exists for weak disorder (low impurity density) and for two dimensions. However, we do not consider transport properties of the system. Instead of being defined by a zero dc conductivity, the nature of the localized states in our approach is defined by the spectral density. The difference between the physics discussed in the scaling approach and the effects, which we discuss here, is the following: In an IB, the electron is localized essentially at one impurity atom, while in case of a short-range random potential, as considered in the scaling approach, the electron is localized in a large number of potential fluctuations.[23] In the scaling theory the driving mechanism for localization is the interference of pairs of waves in the backscattering direction which involves phase coherence of waves scattered by many impurities.[21]

For an interacting electron system a singularity of the DOS at the Fermi energy due to the disorder was predicted.[24–26] This effect is neglected in our theory.

It is well known that the tight-binding coherent-potential approximation can only account for short-range random potentials. However, Klauder's multiple-scattering approach[27] allows the treatment of realistic scattering potentials.

For the three-dimensional systems, the equations in the best Klauder approximation (the fifth approximation) have been solved in Ref. 28. A screened Coulomb potential was used for the electron-impurity interaction. For low impurity concentration a well-defined IB was found. At higher impurity concentrations the IB overlapped with the CB.

Recently it was reported[29] that within a separable potential approximation Klauder's equations are simplified considerably. In this case Klauder's nonlinear integral equation can be reduced to a transcendental algebraic equation for the three-dimensional system. The numerical results of this approach describe the trends of those of the full equations quite satisfactorily.

In this paper we use the fifth Klauder approximation to calculate the density of states in a MOSFET structure in the presence of charged impurities. The impurities are assumed to be screened. Results for weakly screened impurities are also presented. A transition from an IB regime to a BT regime is described. In addition we discuss the separable potential approximation and compare it to the full Klauder solution.

The paper is organized as follows. In Sec. II we define our model and specify the Klauder equations. The results for the DOS for a fully screened potential are discussed in Sec. III. The results for the weakly screened potential are presented in Sec. IV. In Sec. V we use the separable potential approximation to calculate the DOS. In Sec. VI we consider the low impurity limit of our theory and compare it to other theoretical results. Section VII contains a comparison of our theory with experimental results. The conclusion of our paper is presented in Sec. VIII. In the Appendix the Klauder equations are generalized for a distribution of remote impurities.

## II. MODEL AND THEORY

In this section we present the equations and specify our model to calculate the density of states.

### A. The Green function

As usual, we describe the one-electron properties of the interacting electron system by using the one-electron Green function $G(\mathbf{k},E)$, where $\mathbf{k}$ and $E$ are the wave vector and the energy of the quasiparticle, respectively. The Green function is expressed as[30]

$$G(\mathbf{k},E)=\frac{1}{E-\varepsilon(\mathbf{k})-\Sigma(\mathbf{k},E)} . \tag{1}$$

$\varepsilon(\mathbf{k})$ is the kinetic energy of the noninteracting electron system; we use a parabolic dispersion relation with an effective mass $m^*$: $\varepsilon(\mathbf{k})=\hbar^2k^2/2m^*$.

The self-energy $\Sigma(\mathbf{k},E)$ is the sum of exchange and correlation contribution $\Sigma_{xc}(\mathbf{k},E)$ (due to the interaction of the electrons) and the electron-impurity contribution $\Sigma_{e\text{-}i}(\mathbf{k},E)$ (due to the disorder in the system):

$$\Sigma(\mathbf{k},E)=\Sigma_{xc}(\mathbf{k},E)+\Sigma_{e\text{-}i}(\mathbf{k},E) . \tag{2}$$

The self-energy describes the modification of the DOS due to the interaction and to the disorder in comparison to the density of states for the free-electron gas.

The Green function determines the spectral density $A(\mathbf{k},E)$ via

$$A(\mathbf{k},E)=\mp\frac{1}{\pi}\mathrm{Im}G(\mathbf{k},E\pm i0) \tag{3}$$

and the DOS per unit of energy and per unit of volume via

$$\rho(E)=\frac{1}{\Omega}\sum_{\mathbf{k},\sigma}A(\mathbf{k},E) . \tag{4}$$

The summation over $\sigma$ indicates that, in principle, one has a summation over the spin degeneracy $g_s$ and the valley degeneracy $g_v$. $\Omega$ is the volume.

### B. The multiple-scattering approach

We calculate $\Sigma_{e\text{-}i}(\mathbf{k},E)$ in Klauder's best (fifth) multiple-scattering approximation.[27] Serre and Ghazali[28] used a linear transformation to solve the integral equation of Klauder more efficiently for three-dimensional systems. We use the same method in this paper. Details of the method can be found in Ref. 28. The self-energy for the electron-impurity interaction is then determined by

$$\Sigma_{e\text{-}i}(\mathbf{k},E)=U(\mathbf{k},\mathbf{k},E)-N_iV(0) . \tag{5}$$

$N_i$ is the impurity density and $V(\mathbf{q})$ is the electron-impurity interaction potential (the Fourier transform). It is specified in the following subsection of this chapter. In order to calculate $U(\mathbf{k},\mathbf{q},E)$, the following integral equation must be solved:

$$U(\mathbf{k},\mathbf{q},E)=N_iV(\mathbf{k}-\mathbf{q})+\frac{1}{(2\pi)^2}\int d^2q'V(\mathbf{q}'-\mathbf{q})G(\mathbf{q}')U(\mathbf{k},\mathbf{q}',E) . \tag{6}$$

The fifth Klauder approximation can be used to derive the so-called self-consistent Born approximation for the self-energy.[30] In the lowest order, we find with Eq. (6) $U(\mathbf{k},\mathbf{q},E)=N_iV(\mathbf{k}-\mathbf{q})$. If we use this expression on the right-hand side of Eq. (6) we get

$$\Sigma_{e\text{-}i}(\mathbf{k},E)=\frac{N_i}{(2\pi)^2}\int d^2q'\,|V(\mathbf{q}'-\mathbf{k})|^2G(\mathbf{q}') \tag{7}$$

for the self-energy. An analogous equation has been derived by Klauder[27] as his third approximation. The self-consistent Born approximation does not describe IB's and underestimates the disorder effects. This result has been found for three-dimensional systems.[28]

The equations which have been given until now are generally valid for two-dimensional systems. In principle, we can discuss MOSFET systems, heterostructures or quantum wells. In comparison to three-dimensional systems we mention the following. The two-dimensional integral equation in Eq. (6) involves the same numerical expense as the corresponding equation for three-dimensional systems. In this case one integral was evaluated analytically.

### C. The model

We consider an electron gas as realized in a silicon MOSFET system. The wave function $\Psi(z)$ perpendicular to the interface (in $z$ direction) has a finite extension into the bulk and it is characterized for the lowest subband by the variational form [Eq. (3.25) of Ref. 1]

$$\Psi(z)=\left[\frac{b^3}{2}\right]^{1/2}ze^{-bz/2} . \tag{8}$$

The parameter $b$ determines the extension into the bulk. The mean distance between the charge and the oxide-semiconductor interface is given by $\langle z\rangle=3/b$. The electron density $N$ and the depletion density $N_d$ define $b$ via [Eq. (3.30) of Ref. 1]

$$b^3=\frac{48\pi e^2m_z}{\epsilon_{sc}\hbar^2}(N_d+\tfrac{11}{32}N) . \tag{9}$$

$m_z$ is the mass perpendicular to the interface, $e$ is the electron charge and $\epsilon_{sc}$ is the dielectric constant of the semiconductor. The electric field $F$ seen by the two-dimensional electrons also depends on $N$ and $N_d$. In a triangular-well approximation one gets[31]:

$$F=\frac{4\pi e}{\epsilon_{sc}}(N_d+N) . \tag{10}$$

The electron density in the MOSFET structure can be varied by means of the gate voltage. The depletion density depends on the concentration of bulk acceptors and can be varied (for fixed electron density) by a substrate bias. A negative substrate bias (for a $p$-type bulk) increases the depletion density. Inversion layers ($p$-type bulk) have a typical $N_d\sim10^{11}$ cm$^{-2}$. Accumulation layers ($n$-type bulk) have a typical $N_d\sim10^9$ cm$^{-2}$.

We consider an electron-impurity interaction which is screened because of the electron-electron interactions described by the dielectric function $\epsilon(\mathbf{q})$ of the interacting electron gas:

$$V(\mathbf{q})=\frac{V_{e\text{-}i}(\mathbf{q})}{\epsilon(\mathbf{q})} . \tag{11}$$

We assume that the impurities with charge $Ze$ are randomly distributed at the interface of the oxide and the semiconductor. According to the finite extension of the wave function into the bulk, $V_{e\text{-}i}(\mathbf{q})$ is the Coulomb potential for two dimensions with a form factor $F_i(q)$ [Eq. (4.28) of Ref. 1]:

$$V_{e\text{-}i}(\mathbf{q})=\frac{2\pi Ze^2}{\epsilon_L}\frac{1}{q}F_i(q) \tag{12a}$$

and

$$F_i(q)=\frac{1}{(1+q/b)^3} . \tag{12b}$$

The average dielectric constant $\epsilon_L$ is calculated as: $\epsilon_L=(\epsilon_{sc}+\epsilon_{in})/2$. $\epsilon_{in}$ is the dielectric constant of the insulator. $Ze$ is the charge of the impurity. In the random-phase approximation (RPA) with local-field (exchange-correlation) correction, $\epsilon(\mathbf{q})$ is given by[32]

$$\epsilon(\mathbf{q})=1+V_c(q)[1-G(q)]X_0(q) . \tag{13}$$

$V_c(q)$ is the electron-electron interaction potential where finite-extension effects are included

$$V_c(q)=\frac{2\pi e^2}{\epsilon_L}\frac{1}{q}F_c(q) \tag{14a}$$

and [see Eq. (2.52) of Ref. 1]

$$F_c(q)=\frac{1}{2}\left[1+\frac{\epsilon_{in}}{\epsilon_{sc}}\right]\frac{1+\frac{9}{8}q/b+\frac{3}{8}q^2/b^2}{(1+q/b)^3}+\frac{1}{2}\left[1-\frac{\epsilon_{in}}{\epsilon_{sc}}\right]\frac{1}{(1+q/b)^6} . \tag{14b}$$

$X_0(q)$ is the Lindhard function for two dimensions and is expressed as [see Eq. (2.35) of Ref. 1]

$$X_0(q)=\rho_F[1-\Theta(4k_F^2-q^2)(1-4k_F^2/q^2)^{1/2}] , \tag{15}$$

with $\rho_F$ as the density of states of the free electron gas and $k_F$ as the Fermi wave number. For the local-field corrections $G(q)$, we use an analytical function which reproduces approximately the numerical results of Ref. 33:

$$G(q)=\begin{cases}\frac{1}{\pi g_v}\frac{q}{k_F}, & q<2k_F\\ \frac{1}{2g_v}, & q\geq 2k_F .\end{cases} \tag{16}$$

In the Thomas-Fermi approximation the $q$ dependence of $X_0(q)$ is neglected and $G(q)=0$. For the ideally two-dimensional system with $1/b=0$, the screening function in the modified Thomas-Fermi approximation is written as

$$\epsilon(q)=1+\frac{\overline{q_s}}{q} . \tag{17}$$

In Eq. (17) we introduce a screening number $\overline{q_s}=\alpha q_s$ in order to study the screening effect on the DOS. $\alpha$ is a dimensionless parameter. $q_s$ is the Thomas-Fermi wave number, given by the density of states $\rho_F$ or the generalized Bohr radius $a^*$ via $q_s=2\pi e^2\rho_F/\epsilon_L=2g_v/a^*$. In the classical Thomas-Fermi approximation we set $\alpha=1$.

Our impurity-electron potential [Eq. (12)] is the standard potential used in the calculations of transport properties. The cases $b=0$ and $1/b=0$ and the effects on the binding energies will be discussed in Sec. VI B.

Our Eqs. (11)–(17) specify $V(q)$ which enters Eqs. (1)–(6) for the calculation of the self-energy $\Sigma_{e\text{-}i}(\mathbf{k},E)$. For the exchange-correlation contribution to the self-energy, various approximations have been discussed in the literature.[1] The energy dependence of $\Sigma_{xc}$ is a weak one. The $\mathbf{k}$ dependence of the exchange contribution $E_{ex}$ nearly compensates for the $\mathbf{k}$ dependence of the correlation contribution $E_c$. We approximate the numerical results of Vinter[34] for $k=k_F$ by the following analytical expression

$$\Sigma_{xc}(k_F,E)=E_{ex}+E_c , \tag{18a}$$

with

$$E_{ex}=-0.710R\,(Na^{*2})^{0.428} , \tag{18b}$$

$$E_c=-0.122R . \tag{18c}$$

Because $\Sigma_{xc}(k_F,E)$ is real, it produces a rigid shift of the band in comparison to the band of the free-electron gas.

In this paper we have solved the equations for Si(100) MOSFET systems with $m^*=0.19m_0$, $m_z=0.916m_0$, $\epsilon_{sc}=11.5$, $\epsilon_{in}=3.9$, $g_v=2$, and $g_s=2$. $m_0$ is the vacuum mass of the electron. Our results are, however, more general. This is due to the fact that the natural length scale in our system is the Bohr radius $a^*=\epsilon_L\hbar^2/m^*e^2$. The screening wave number is given by $q_sa^*=2q_v$. The natural energy scale is the effective Rydberg $R=m^*e^4/2\epsilon_L^2\hbar^2$. For the silicon (100) MOSFET we have $a^*=21.45$ Å and $R=43.6$ meV. Because of the natural scales, we present our results in these units. The density of states is presented in units of $\hat{\rho}=1/2\pi Ra^{*2}$. For the free-electron gas we have $\rho=g_v\hat{\rho}$. For Si(100) the unit of the DOS is $\hat{\rho}=7.93\times10^{13}$ eV$^{-1}$ cm$^{-2}$. In the following the energy of the lowest subband is set to $E=0$.

## III. RESULTS FOR THE FULLY SCREENED POTENTIAL

In this section we present our results for the DOS in the Klauder approximation and in the case in which the RPA [Eq. (13)] is used for the screening. The RPA is certainly valid for high $N$. However, we believe that it describes at least qualitatively the DOS for low electron densities. In Sec. III A we discuss the DOS and in Sec. III B the spectral density is considered.

### A. The density of states

The DOS depends via Eqs. (4)–(6) on the impurity density. The electron density and the depletion density determine the parameter $b$, and $b$ modifies the electron-impurity potential in Eq. (11). The electron density also modifies the screening function, Eq. (13), for finite $q$ via the Fermi wave number.

We have solved the integral equation defined in Eqs. (1), (2), (5), (6), and (11) with impurities at the oxide-semiconductor interface [Eq. (12)] using the RPA screening function [Eq. (13)]. In Fig. 1 we show the DOS according to Eq. (4) versus energy for fixed electron and depletion densities ($N=2\times10^{11}$ cm$^{-2}$ and $N_d=3\times10^{11}$ cm$^{-2}$) and for different values of $N_i$. For high impurity concentrations the CB exhibits a BT at low energies. For

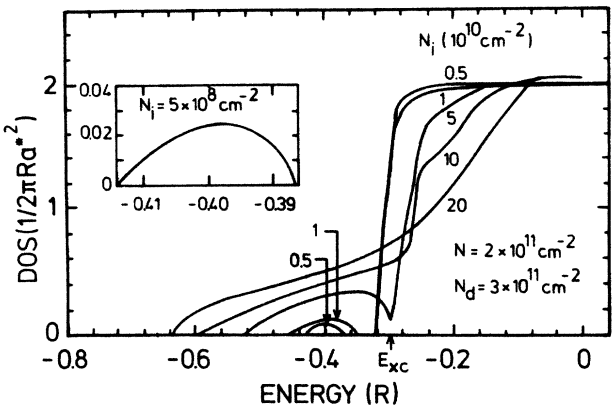


FIG. 1. Density of states (DOS) versus energy ($E$) for different impurity densities ($N_i$) according to the Klauder approximation and the random-phase approximation.

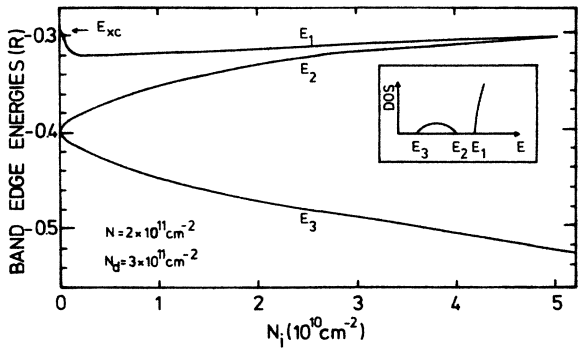


FIG. 2. Band-edge energies (as indicated in the inset) versus impurity concentration according to the Klauder approximation and the random-phase approximation.

high energies the DOS of the free electron gas is reached. As $N_i$ decreases the BT shrinks, and for $N_i < 5\times10^{10}$ cm$^{-2}$ an IB split off from the CB by an energy gap is formed. The shift of the CB due to the electron-electron interactions ($\Sigma_{xc}$) is of the same order of magnitude as the effects due to disorder ($\Sigma_{e\text{-}i}$), which are responsible for the IB or the BT for $E < E_{xc}$. For $N_i = 0$ the density of states is given by $\rho(E) = g_v \hat{\rho} \Theta(E - E_{xc})$ and $\Theta(x)$ is the step function. A disappearance of the IB was also found in three-dimensional systems.[28] The impurity concentration $\tilde{N}_i$, where the IB disappears, is characterized by the dimensionless number $f_d$ for a $d$-dimensional system, defined by $\tilde{N}_i^{1/d} a^* = f_d$. For three dimensions with $N = N_i$, $f_3 = 0.12$ was found. Our $\tilde{N}_i = 5\times10^{10}$ cm$^{-2}$ corresponds to $f_2 = 0.05$. This number depends, however, on $N$ and $N_d$.

It is obvious from Fig. 1 that the states in the IB stem from the edge of the CB. The width of the IB is already significant at the lowest impurity concentration which can be reached experimentally ($1\times10^{10}$ cm$^{-2}$). We have verified that the number of states in the IB between its edges $E_3$ and $E_2$ is indeed given by

$$\int_{E_3}^{E_2} \rho(\varepsilon) d\varepsilon = g_s g_v N_i \ . \tag{19}$$

In Fig. 2 the CB edge and the IB edges versus impurity concentration are shown. For $N_i \to 0$, the energy of the impurity level is located at $-0.4R$; the binding energy $E_B$ is $0.1R$. The width of the IB increases with increasing impurity concentration. A similar behavior as in Fig. 2 was found in three-dimensional systems.[28] In this case the impurity dependence of the band-edge energies is stronger because the electron density has been varied according to $N = N_i$. In Fig. 2 the same parameters as in Fig. 1 have been used for $N$ and $N_d$.

In Fig. 3 the energy dependence of the DOS for fixed $N$ and $N_i$ and three values of $N_d$ are shown. For $N_d = 0$ (accumulation) we find a band tail, while for $N_d = 6\times10^{11}$ cm$^{-2}$ an IB is found. With increasing $N_d$ the electron wave function is pushed to the interface, the electron-impurity interaction becomes more ideally two-dimensional, and the binding energy of the bound state increases. This will be discussed in more detail in Sec. VI. For $N_d = 0$ the impurity concentration ($N_i = N = 1\times10^{11}$ cm$^{-2}$) is already high enough to produce a BT. For $N_d = 3\times10^{11}$ cm$^{-2}$ an IB is found, which is, however, not split off from the CB. From the split-off IB for $N_d = 6\times10^{11}$ cm$^{-2}$ we estimate that $f_2 = 0.07$ instead of 0.05 as found in Fig. 1 for some other $N$ and $N_d$.

The DOS versus energy for $N_i = 1\times10^{11}$ cm$^{-2}$, $N_d = 3\times10^{11}$ cm$^{-2}$ and three different electron densities is shown in Fig. 4. The increase of $N$ increases the binding energy via the confinement parameter $b$. Yet according to the parameters used in Fig. 4 this effect is small; see Eq. (9). The increase of $N$ also increases the screening properties; see Eq. (13). This is why an IB becomes a BT with increasing electron density, shown in Fig. 4.

For every electron density we used the DOS versus energy according to Fig. 4 to calculate the DOS at the Fermi level. This DOS versus electron density is shown in the inset of Fig. 4, where we used a degeneracy of $g_s g_v = 1$. The non-split-off IB in the DOS versus energy as seen in Fig. 4 is reflected in the DOS versus electron density.

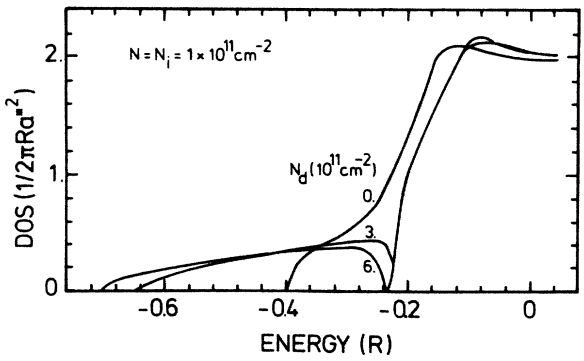


FIG. 3. Density of states versus energy for three different depletion densities ($N_d$) according to the Klauder approximation and the random-phase approximation.

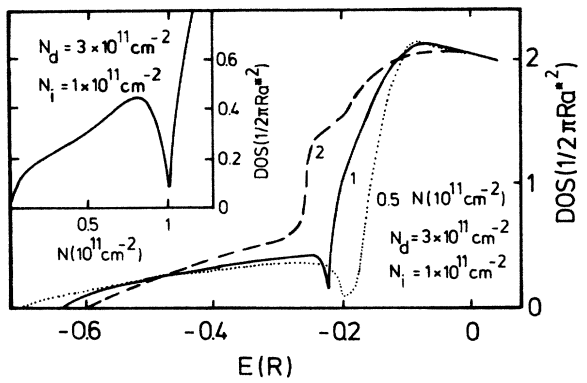


FIG. 4. Density of states versus energy for three different electron densities according to the Klauder approximation and the random-phase approximation. The inset shows the density of states at the Fermi energy versus electron density.

### B. The spectral density

In order to get some information on the spatial behavior of the electron wave function, we consider the spectral density; see Eq. (3). $A(k,E)$ measures the probability that the electron with energy $E$ is in a state with wave number $k$. In Fig. 5 we show an example for $N=2\times10^{11}$ cm$^{-2}$ and $N_d=3\times10^{11}$ cm$^{-2}$.

For $N_i=1\times10^{10}$ cm$^{-2}$, as in Fig. 5(a), a split-off IB exists; see also Fig. 1. In the CB ($E=0$) the spectral density peaks at a finite $k$ and the width $\Delta k$ is very narrow. In the IB ($E=0.4R$) the peak is at $k=0$ and the width is very large. According to the uncertainty equation $\Delta\mathbf{k}\cdot\Delta\mathbf{r}=$constant we conclude that in the first case the state is extended in real space, while in the IB the state is localized in space.

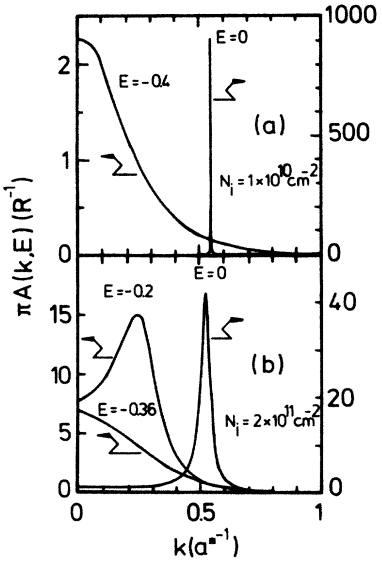


FIG. 5. Spectral density [$A(k,E)$] for typical energies versus wave number ($k$) for $N=2\times10^{11}$ cm$^{-2}$ and $N_d=3\times10^{11}$ cm$^{-2}$ and for two different impurity concentrations according to the Klauder approximation and the random-phase approximation.

As in Ref. 28 we define the ratio $r=A(k=0,E)/A(k_m,E)$, where $k_m$ is the value of $k$ for which $A(k,E)$ has a maximum. In Fig. 5(a) we find $r=0$ for the state in the CB and $r=1$ for the state in the IB.

For $N_i=2\times10^{11}$ cm$^{-2}$, as in Fig. 5(b), we are in a BT situation, see Fig. 1. For $E=-0.36R$, $E=-0.2R$, and $E=0$, we get $r=1$, $r=0.51$, and $r=0.024$, respectively. As in $d=3$ we find, starting from the band edge, successively localized, hybrid, and extended states as the energy increases.

In order to calculate the density of states at the Fermi level one has to know the spin and valley degeneracy of the IB or the BT. In the IB regime we expect an impurity to be able to bind only one electron ($g_s=1$). The IB is full for $N=N_i$ and for temperature zero if we assume $g_v=1$. In the CB we expect $g_sg_v=4$. Therefore we believe that $g_sg_v$ varies from 1 to 4 when the Fermi energy goes from the IB to the CB. Because our electron-impurity potential does not depend on the spin or the valley degeneracy, the problem of the degeneracy of the DOS cannot be solved.

## IV. RESULTS FOR THE WEAKLY SCREENED POTENTIAL

In this section we present our results for the DOS in the Klauder approximation in the case of the modified Thomas-Fermi approximation [Eq. (17)] being used for the screening. We expect this approximation with $\bar{q}_s\to0$ to be realistic for $N\to0$ (the Fermi energy is in the IB).

### A. The influence of the screening parameter

The experimental results on the sodium-doped silicon MOSFET system[2-4] indicate that the electrons in the IB are localized. The temperature dependence of the conductivity in the IB has been fitted with a single-particle hopping model for noninteracting electrons.[4]

In case of localized electrons we expect the screening behavior to change substantially in comparison to the screening behavior of free electrons. However, a qualitative theory for the screening properties of localized electrons in an IB is not available from the literature in two dimensions. One expects that for localized electrons the screening function for $q\to0$ is finite as in an insulator.[35,36]

For these reasons we have studied the Klauder approximation within the modified Thomas-Fermi approximation given in Eq. (17). The screening wave number $\bar{q}_s$ was reduced by a factor of 80 in comparison to the value of the free electron gas. Because of the singular nature of the unscreened potential for $q\to0$, we were not able to solve Eq. (6) with an unscreened electron-impurity interaction ($\bar{q}_s=0$). We believe, however, that the reduction of the screening wave number simulates a weakly screened potential. We will present further arguments regarding this point in Sec. V.

In Fig. 6 we have plotted the DOS versus energy for $N=2\times10^{11}$ cm$^{-2}$, $N_i=1\times10^{11}$ cm$^{-2}$, $N_d=3\times10^{11}$ cm$^{-2}$, and for various screening parameters $\bar{q}_s=\alpha q_s$. For $\alpha=1$ (the full screening in the modified Thomas-Fermi

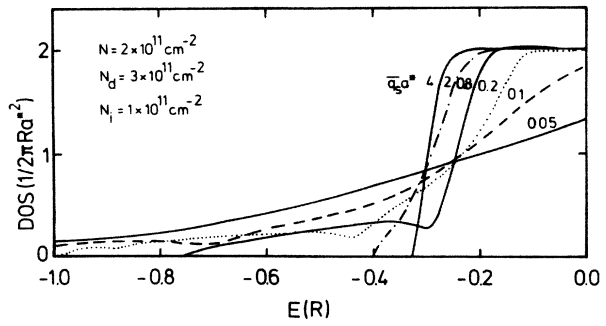


FIG. 6. Density of states versus energy for different screening parameters $\bar{q}_s$ according to the Klauder approximation and the modified Thomas-Fermi approximation.

approximation) we find no IB and the CB starts at $-0.33R$, which corresponds roughly to the shift of the band due to $E_{xc}$. With decreasing $\alpha$ (decreasing screening) the CB edge moves to lower energy.

For $\alpha=0.05$ some peaks in the DOS are observable for low energies. For $\alpha<0.0125$ these peaks disappear again and the DOS becomes smooth. The origin of these peaks are excited IB's; this will be discussed below. From Fig. 6, however, it becomes understandable that a screened potential underestimates the shift of the CB edge due to disorder.

### B. The excited impurity bands

The disappearance of the structures in the DOS in Fig. 6 for $\alpha<0.0125$ motivated us to study this effect in some detail. In Fig. 7 the DOS versus energy is shown for $N=2\times10^{11}$ cm$^{-2}$, $N_d=3\times10^{11}$ cm$^{-2}$, $\alpha=0.025$, and for various impurity concentrations. The curve with $N_i=1\times10^{11}$ cm$^{-2}$ was also shown in Fig. 6. With decreasing impurity concentration the structure in the DOS for $E<E_{xc}$ reappears, and for $N_i=5\times10^{9}$ cm$^{-2}$ we identify three IB's at the energies $-0.85R$, $-0.48R$, and $-0.034R$. The exchange-correlation contribution to the self-energy is $E_{xc}=-0.295R$.

The origin of the disappearance of the structure at the low-energy tail of the DOS in Fig. 6 for $\alpha<0.025$ is interpreted according to Fig. 7 as follows: With decreasing $\alpha$ the ground state of the IB shifts to lower energy and additional excited IB's are shifted from the CB into the energy range of the bound states ($E<E_{xc}$). With a further decrease of $\alpha$ the IB's become broader and the overlapping of the different IB's and of the CB results in a monotonic energy dependence of the DOS. As for the fully screened potential (Fig. 2), Fig. 7 shows that for $\alpha=0.025$ the overlapping begins for $N_i=5\times10^{10}$ cm$^{-2}$. Although the weakly screened potential is stronger than the potential screened within the RPA, the critical impurity concentration to obtain a split-off IB does not change dramatically due to the existence of overlapping excited IB's.

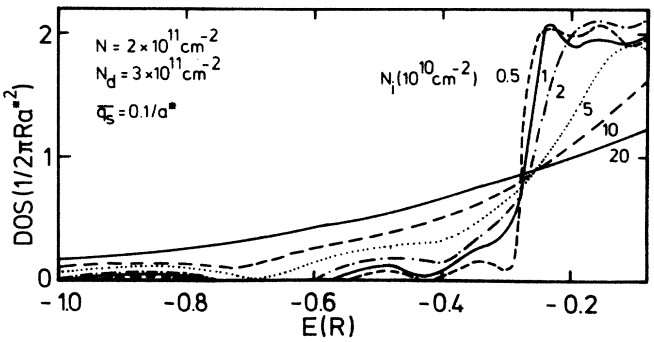


FIG. 7. Density of states versus energy for different impurity densities according to the Klauder approximation and the modified Thomas-Fermi approximation.

For a complete description of the system, a self-consistent calculation of the screening behavior and of the DOS would be necessary. Therefore a complete theory for the metal-insulator transition must be available. This is not the case. Given this theory, one should expect the screening properties of the electrons to change from insulating to metallic if the Fermi energy increases. We believe our theory with $\alpha=1$ (full screening) to be realistic if the Fermi energy is greater than $E_{xc}$. Our results for a weakly screened potential ($\alpha\to0$) are more realistic if the Fermi energy is much smaller than $E_{xc}$.

## V. RESULTS FOR THE SEPARABLE POTENTIAL APPROACH

In this section we discuss the fifth Klauder approximation assuming that the electron-impurity interaction potential is a separable potential. The good qualitative agreement between the separable potential approximation and the Klauder approximation for three-dimensional systems[29] motivated us to study this approach for two-dimensional systems; especially because the numerical effort for the separable potential approximation is much lower than for the Klauder approximation. Furthermore the limit $N_i\to0$ can be studied analytically in the sense that the binding energy can be calculated within this approach. We found, however, some features in the separable potential approximation, which we did not expect from our calculation within the Klauder approximation and which we attribute to the separable potential approximation.

### A. Theory

The essential assumption of the separable potential approximation is that the electron-impurity interaction potential can be written as

$$V(\mathbf{q}-\mathbf{q}')=ZC(d)V^{1/2}(q)V^{1/2}(q')\ . \tag{20}$$

The dimensionless parameter $C(d)$ determines the energy of a bound state for $N_i\to0$ for the $d$-dimensional system and will be determined later. It is obvious that the separable potential approximation is exact for a $q$-independent electron-impurity potential (zero range potential in normal space). With Eq. (20) we can solve Eq. (6) and get

$$U(\mathbf{k},\mathbf{q},E)=ZC(d)V^{1/2}(k)V^{1/2}(q)\frac{B(E)}{1-ZB(E)}\ . \tag{21}$$

According to Eq. (5) the self-energy $\Sigma_{e\text{-}i}(\mathbf{k},E)$ can then be expressed as a product of a $k$-dependent function (the electron-impurity potential) and an energy-dependent function

$$\Sigma_{e\text{-}i}(k,E)=Z^2C(d)V(k)N_i\frac{B(E)}{1-ZB(E)}\ , \tag{22a}$$

with

$$B(E)=\frac{C(2)}{2\pi}\int_0^\infty dq\, qV(q)G(q,E) \tag{22b}$$

for $d=2$.

For a three-dimensional system the function $B(E)$ can be calculated analytically within the Thomas-Fermi approximation for the screening.[29] In our case, however, because of the form factor $F_i(q)$, we have to solve $B(E)$ numerically. We can also study numerically the influence of the various approximations on the screening function (RPA, modified Thomas-Fermi approximation) and we can use various approximations for the electron-impurity interaction potential.

The function $B(E)$ depends via $G(\mathbf{q},E)$ on the impurity density. In the limit $N_i\to 0$, for $1/b=0$ (ideally two-dimensional system) and for an unscreened potential, $B(E)$ which we denote by $B^0(E)$ is given by

$$B^0(E)=C(d)\frac{e^2}{\epsilon_L}\int_0^\infty dq\frac{1}{E-q^2/2m} \tag{23}$$

for $Z=-1$. For $E<0$ we find explicitly

$$B^0(E)=-\pi C(2)\frac{1}{(E/R)^{1/2}}\ . \tag{24}$$

According to Eq. (22a) we expect a bound state when $1-ZB^0(E)=0$ is fulfilled. For an ideally two-dimensional system the bound state is at $-4R$. With Eq. (24) we conclude that

$$C(2)=2/\pi \tag{25}$$

to reproduce a bound state at $-4R$ within the separable potential approximation and for $Z=-1$. For three-dimensional systems the parameter $C(3)$ was determined in Ref. 29: $C(3)=\frac{1}{2}$.

In the following part of this section we discuss the separable potential approximation for $d=2$ and compare it with the results of the Klauder approximation.

### B. The full screened potential

In this subsection we discuss our results for the separable potential approximation [Eq. (22)] and the electron-impurity interaction potential according to Eq. (11). For the screening we use the RPA [Eq. (13)].

For $N=N_i=1\times10^{10}\ \mathrm{cm}^{-2}$ and $N_d=3\times10^{11}\ \mathrm{cm}^{-2}$ the DOS versus energy is shown in Fig. 8. The solid curve corresponds to the Klauder approximation and the dashed curve corresponds to the separable potential approximation. The separable potential approximation describes the IB quite well; the energy range and the width of the IB are in reasonable agreement with the Klauder approximation where the RPA was used. We believe that

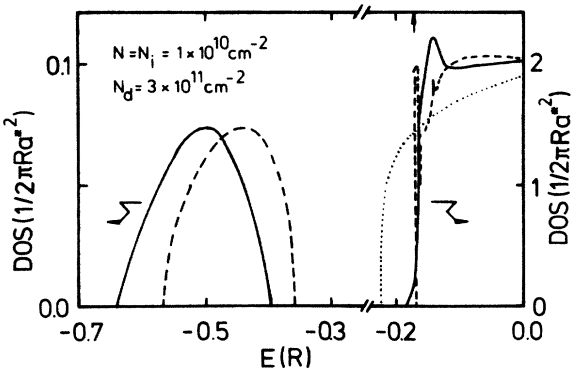


FIG. 8. Density of states versus energy within the random-phase approximation. The solid and the dashed lines corresponds to the Klauder approximation and the separable potential approximation, respectively. The dotted line corresponds to Eq. (7).

the structures on the CB edge in the separable potential approximation are due to the approximation involved in this approach. The dotted line in Fig. 8 results from the self-consistent Born approximation [Eq. (7)]. However, the $q$-dependence of the self-energy was neglected: $\Sigma_{e\text{-}i}(\mathbf{k},E)=\Sigma_{e\text{-}i}(0,E)$. The numerical effort for this simplified self-consistent Born approximation is the same as for the separable potential approximation.

We have also studied the influence of the screening on the DOS for the same parameters as in Fig. 8. Within the Thomas-Fermi approximation (modified Thomas-Fermi approximation, $\alpha=1$) we did not find an IB in the Klauder approximation. The same result was observed within the separable potential approximation. The $q$-dependence of the screening function in the RPA is responsible for this behavior. Since we did not find a significant change in the IB neglecting local-field corrections in the RPA, we conclude that the $q$-dependence of the Lindhard function [Eq. (15)] is most important for the existence of the IB.

The band structure is characterized by the CB edge and the two edges of the IB; see the inset in Fig. 9. The

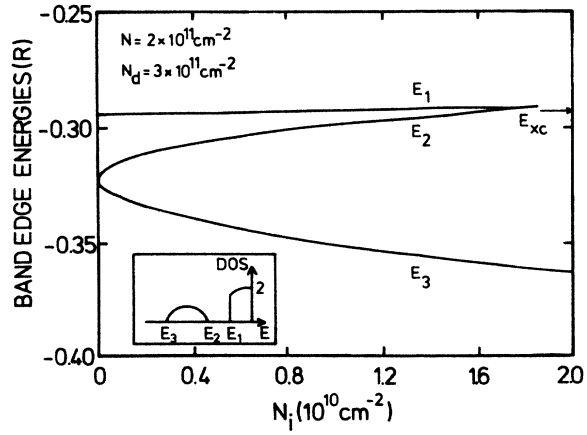


FIG. 9. Band-edge energies (as indicated in the inset) versus impurity density according to the separable potential approximation and the random-phase approximation.

dependence of the band edge energies versus impurity density for $N=2\times10^{11}$ cm$^{-2}$ and $N_d=3\times10^{11}$ cm$^{-2}$, as in Fig. 2, is shown in Fig. 9. A split-off IB is found for $N_i<\tilde{N}_i=1.8\times10^{10}$ cm$^{-2}$. For $N_i\to0$ we find the impurity level at $0.027R$ below the CB. In the Klauder approximation the impurity level is found at $0.1R$ below the CB (see Fig. 2). Thus we only found qualitative agreement between the separable potential approximation and the Klauder approximation. The binding energy (for $N_i\to0$) and $\tilde{N}_i$ depend on $N$. For $N=1\times10^{11}$ cm$^{-2}$ and $N_d=3\times10^{11}$ cm$^{-2}$ we found in the separable potential approximation a split-off IB for $N_i<\tilde{N}_i=5\times10^{10}$ cm$^{-2}$ and the bound state for $N_i\to0$ is observed at $0.076R$ below the CB.

The width $\Gamma$ of the IB is well described by

$$\Gamma=\Gamma_0\left[\frac{N_i}{10^{10}\text{ cm}^{-2}}\right]^{1/2}, \tag{26}$$

where the prefactor $\Gamma_0$ depends on $N$ and $N_d$. The $N_i$ dependence is in agreement with the coherent potential approximation (CPA) results.[37] For $N=2\times10^{11}$ cm$^{-2}$ and $N_d=3\times10^{11}$ cm$^{-2}$ we find $\Gamma_0=0.051R$, while for $N=1\times10^{11}$ cm$^{-2}$ and $N_d=3\times10^{11}$ cm$^{-2}$ we find $\Gamma_0=0.090R$. For these values of $N$ and $N_d$ the extension parameter $b$ is not very different in the two given cases. The origin of the different $\Gamma_0$ must then be screening differences due to the different electron densities.

Within the Klauder approximation our numerical results for the width of the IB (Fig. 2) can also be fitted by the Eq. (26). For $N=2\times10^{11}$ cm$^{-2}$ and $N_d=3\times10^{11}$ cm$^{-2}$ we get $\Gamma_0=0.110R$. A similar equation as Eq. (26) also holds for the maximum of the DOS in the IB: $\rho_m\propto N_i^{1/2}$, in agreement with the CPA result.[37]

### C. The weakly screened potential

The modified Thomas-Fermi approximation [Eq. (17)] can be studied in the separable potential approximation too. The advantage of the separable potential approximation in comparison to the Klauder approximation is that the limit $\bar{q}_s=0$, i.e., the completely unscreened Coulomb potential, can also be discussed. For this reason we consider it worthwhile to study the separable potential approximation in the limit $\alpha\to0$ in some detail.

If we reduce $\alpha$ from 1 to 0 we qualitatively find the following behavior for the DOS. With decreasing $\alpha$ the IB shifts to lower energy and becomes broader. There is a drastic shift for $\alpha$ between 1 and 0.01. For $\alpha<0.01$, it seems that the lower band edge goes to very low energies and the IB is very broad. However, the DOS at very low energies is small. The long tail in the DOS is certainly due to the long-ranged nature of the unscreened potential. The upper band edge of the IB and the energy where the DOS in the IB is maximum are no longer varying for $\alpha<0.01$ and go to finite values for $\alpha\to0$. A qualitatively similar result has been found in the Klauder approximation (see Fig. 6). The impurity concentration $\tilde{N}_i$ where the IB merges with the CB also increases drastically with decreasing $\alpha$, in disagreement with the Klauder approximation. This behavior stems from the fact that in the separable potential approximation we did not find excited IB's (for $\alpha\to0$), while in the Klauder approximation the excited IB's fill the gap in the DOS between the lowest IB and the CB.

On the CB edge we found an increase of the DOS with decreasing $\alpha$. We expect that this behavior is also a defect of the separable potential approximation.

In Fig. 10 the band edges (as indicated in the insert) versus impurity concentration for $N=2\times10^{11}$ cm$^{-2}$, $N_d=2\times10^{11}$ cm$^{-2}$ and the unscreened electron-impurity potential ($\alpha=10^{-6}$) are shown. Comparing Figs. 9 and 10 we observe that the energy of the bound state for $N_i\to0$ goes from $E_B=0.03R$ in the screened case to $E_B=0.6R$ in the unscreened case. $\tilde{N}_i$ changes from $1.8\times10^{10}$ cm$^{-2}$ in the screened case to $5\times10^{11}$ cm$^{-2}$ in the unscreened case. We conclude that, without a detailed knowledge of the screening behavior in the IB, a definite conclusion on $\tilde{N}_i$ cannot be reached. The width of the IB in Fig. 10 does not depend significantly on $N_i$ for $N_i>0.5\times10^{11}$ cm$^{-2}$ and the width is of the same order of magnitude as the energy of the bound states for $N_i\to0$.

Because of the satisfying agreement of the binding energy in the limit $N_i\to0$ with exact calculations (see Sec. VI), we have used the separable potential approximation to calculate the DOS versus electron density. For an unscreened potential and $N_d>N$ the DOS versus energy is nearly independent of $N$. The reason is that the potential is only determined by $b$. In Fig. 11 we have shown the DOS versus electron density for $N_d=3\times10^{11}$ cm$^{-2}$ and $N_i=3\times10^{11}$ cm$^{-2}$. First we calculated the DOS versus energy for $N=1\times10^{11}$ cm$^{-2}$ and then we filled the IB with electrons up to the Fermi level. For the left-hand and the lower scales in Fig. 11 a degeneracy of $g_sg_v=4$ was assumed, while we used $g_sg_v=1$ for the right-hand and the upper scales. The DOS versus density is very similar to the result which we have shown in the inset of Fig. 4.

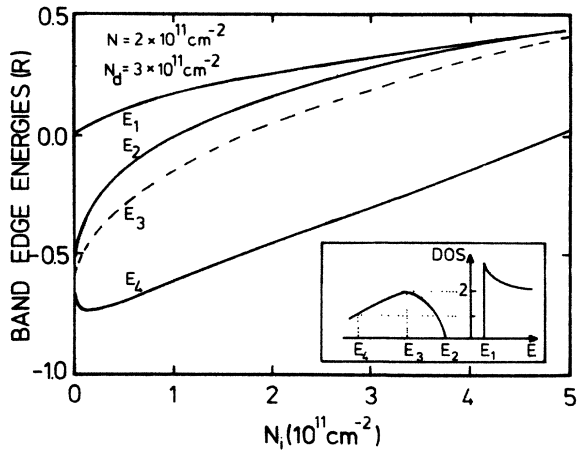


FIG. 10. Band-edge energies (as indicated in the inset) versus impurity density according to the separable potential approximation and the modified Thomas-Fermi approximation with $\alpha=10^{-6}$ ($E_{xc}=0$).

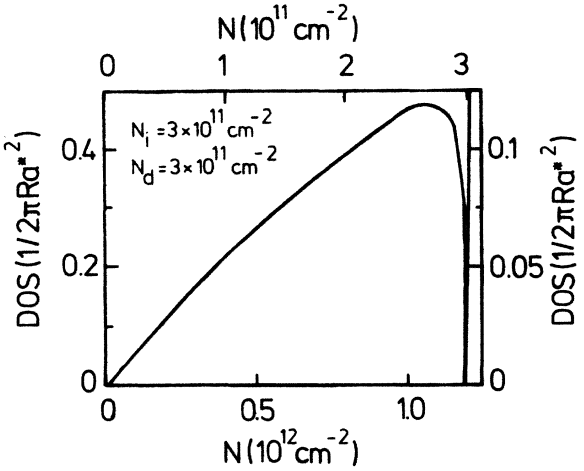


FIG. 11. Density of states at the Fermi energy versus electron density according to the separable potential approximation and the modified Thomas-Fermi approximation for $\alpha=10^{-6}$ ($E_{xc}=0$). The scale on the left-hand side and the lower scale correspond to $g_s g_v=4$. The right-hand side and the upper scales correspond to $g_s g_v=1$.

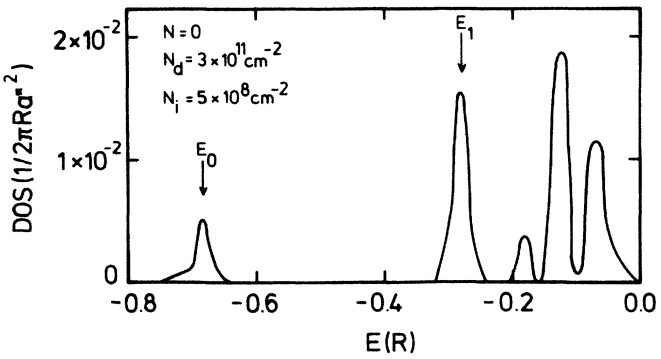


FIG. 12. Density of states versus energy according to the Klauder approximation and the modified Thomas-Fermi approximation for $\bar{q}_s a^*=0.075$ ($\alpha=0.019$). $E_0$ and $E_1$ indicate the energy of the bound state and the first excited bound state, respectively ($E_{xc}=0$).

In connection with the separable potential approximation we mention the following: Our approaches for a fully screened and for a completely unscreened potential must be considered as two relevant physical limits. However, we have not found a criterion to test the quality of the separable potential approximation in case of an unscreened potential. Therefore we believe that these results must be considered with caution.

## VI. THE LOW-IMPURITY-DENSITY LIMIT

In order to compare our theory with exact results, we have calculated the DOS in the limit of very small impurity concentrations.

### A. The Klauder approach

The binding energy of an unscreened electron bound to a charged impurity has been calculated by solving the Schrödinger equation.[6–13] In order to compare these results with our theory we have studied the DOS versus energy for $N_i=5\times10^8$ cm$^{-2}$ and $N_d=2\times10^{11}$ cm$^{-2}$ within the modified Thomas-Fermi approximation. The screening parameter $\alpha$ has been reduced to $\alpha=0.0125$. For $\alpha<0.01$ we got numerically uncertain results, because the impurity potential becomes more singular for $q\to0$. The calculations are done for $N=0$. Let us mention that the binding energy does depend on $N$ via the parameter $b$. However, we know, from the separable potential approximation that the shift of the IB with decreasing $\alpha$ is small for $\alpha<0.01$. In Fig. 12 the DOS for $\bar{q}_s a^*=0.075$ versus energy for $E<0$ is shown. $E_0$ indicates the ground state IB, $E_1$ indicates the first excited IB. We have studied the energy of these two IB's as functions of $\alpha$. The results are given in Table I. For the two lowest values of $\alpha$ a saturation of $E_0$ and $E_1$ is obtained. Then the lowest values of $\alpha$ give a good estimate of $E_0$ and $E_1$ for the fully unscreened potential ($\alpha=0$). Vinter[11] found $-0.69R$ for the $E_0$ state and $-0.29R$ for the $E_1$ state for $N_d=2\times10^{11}$ cm$^{-2}$. The agreement between these values and our values for $\bar{q}_s a^*=0.05$ is satisfactory.

From Fig. 12 we see that between the CB edge (here at $E=0$ because we used $E_{xc}=0$) and $E_1$ additional bound states exist. Unfortunately only the two lowest bound states have been discussed in the single-impurity approach. Therefore we cannot compare the binding energies of our additionally excited bound states (IB's) with other theoretical work.

In order to get further information on the nature of the excited IB's we have calculated the spectral density. The parameter $r$, which we have introduced in Sec. III B, indicates in a certain way that all states in the various impurity levels are localized. We found for the IB's shown in Fig. 12 the following values for $E/r$: $-0.08R/1$, $-0.12R/0.52$, $-0.18R/1$, $-0.28R/0.58$, and $-0.68R/1$. For $E=-0.08R$ we found a node in the spectral density at $ka^*=0.15$ and a relative maximum at $ka^*=0.3$. According to our discussion in Sec. III B the electrons in the excited IB's still have an atomiclike character. We believe that further theoretical studies could lead to a better understanding of the spectral density.

### B. The separable potential approach

In the separable potential approximation the bound-state energy can be calculated without solving the full equation for the self-energy. In Sec. V A we used the se-

TABLE I. Energies $E_0$ and $E_1$ (as indicated in Fig. 12) for $N_i=5\times10^8$ cm$^{-2}$, $N_d=2\times10^{11}$ cm$^{-2}$, $N=0$, and for different screening parameter values.

| $\bar{q}_s$ (units of $1/a^*$) | $\alpha$ | $E_0$ (units of $R$) | $E_1$ (units of $R$) |
|---|---|---|---|
| 0.20 | 0.05 | −0.30 | −0.04 |
| 0.10 | 0.025 | −0.50 | −0.18 |
| 0.075 | 0.019 | −0.68 | −0.28 |
| 0.05 | 0.0125 | −0.72 | −0.32 |

parable potential approximation in the limit $N_i \to 0$ to determine $C(2)$ [see Eq. (23)] for a $1/q$ potential. The argument can be generalized by using realistic potentials. The bound-state energy $E_B$ for $N_i \to 0$ is defined by

$$1 - ZB^0(E_B) = 0 \ . \tag{27a}$$

Here $Z = -1$, and $B^0(E)$ is given by

$$B^0(E) = \frac{1}{\pi^2} \int_0^\infty dq \, qV(q) \frac{1}{E - q^2/2m} \ . \tag{27b}$$

In case of an unscreened potential with finite thickness effects [see Eq. (12)], the binding energy is expressed by

$$E_B = x(ba^*)^2 R \tag{28a}$$

and $x$ is determined by

$$ba^* = \frac{2}{\pi} \frac{1}{(1+x)^3} \left[ (x-3)(-3-\ln x + x) + (12x-4)\left[1 - \frac{\pi}{4}\frac{1}{\sqrt{x}}\right]\right] \ . \tag{28b}$$

The parameter $b$ was defined in Eq. (9) and depends on $N$ and $N_d$. The binding energy versus $N_d$ and $N = 0$ corresponds to the dotted line in Fig. 13. For $N_d \to \infty$ ($b \to \infty$) the binding energy goes to $4R$, the binding energy of the $1s$ state in the ideally two-dimensional system. For $N_d \to 0$ ($b \to 0$) our binding energy goes to zero. This behavior is a drawback of our model. For $b \to 0$ the electron-impurity interaction potential also goes to zero due to the fact that the parameter $b$ was calculated within a variational method. The correct limit for the binding energy for $b \to 0$ is $E_B = 0.25R$.

Phenomenologically we argue that we must replace Eq. (12b) by

$$F_i(q) = \frac{1}{(1+q/b^*)^3} \ , \tag{29a}$$

with

$$b^* = b + b_{2p} \ . \tag{29b}$$

For $b \to 0$ the effective thickness parameter $b^*$ goes to $b_{2p}$. We define $b_{2p}$ via $\langle z^2 \rangle_1 = \langle z^2 \rangle_2$. The average $\langle z^2 \rangle_1$ is defined by the wave function given in Eq. (8) with $b = b_{2p}$. The average $\langle z^2 \rangle_2$ is defined by the hydrogen wave function of a $2p$ state $\Psi(r,\theta,\phi) \propto re^{-r/2a^*}\cos\theta e^{im\phi}$. We get $\langle z^2 \rangle_1 = 12/b_{2p}^2$ and $\langle z^2 \rangle_2 = 18a^{*2}$; then $b_{2p}$ is given by

$$b_{2p} = 0.6/a^* \ . \tag{30}$$

The binding energy according to Eq. (28) and to the effective thickness parameter $b^*$ according to Eq. (29b) as function of $N_d$ for $N = 0$ represents the solid curve in Fig. 13. The theoretical results of Lipari,[9] Martin and Wallis,[10] and Vinter[13] are also shown. These results are in satisfactory agreement with our theoretical results. In Refs. 9 and 10 the binding energy versus an external electric field was evaluated. We used Eq. (10) with $N = 0$ to relate $N_d$ and $F$; see the upper scale of Fig. 13.

In all our calculations of the DOS we have used Eq. (12) for the electron-impurity interaction potential. Comparing the dotted line with the results of Refs. 9, 10, and 12 we see that for inversion layers with $N_d \sim 10^{11}$ cm$^{-2}$ the quantitative agreement is satisfactory. For accumulation layers with $N_d \sim 10^9$ cm$^{-2}$ our binding energies are

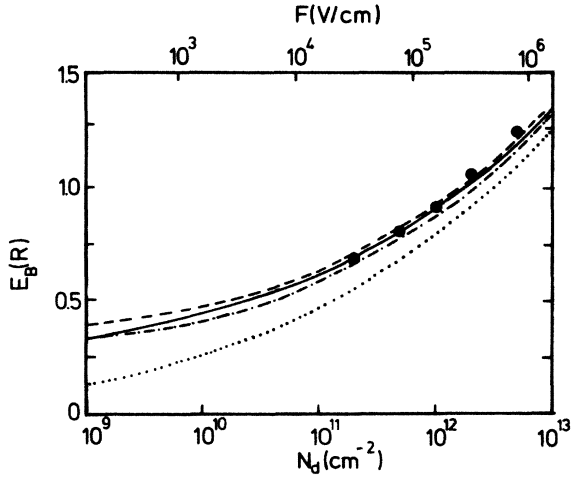


FIG. 13. Binding energy versus depletion density according to the separable potential approximation and the modified Thomas-Fermi approximation for $\alpha = 0$ and for $N = 0$. The full line according to Eq. (28) with $b = b^*$, which is given in Eq. (29b). The dotted line according to Eq. (28) with $b$ given in Eq. (9). The dashed and the dashed dotted lines according to Refs. 9 and 10, respectively. The dots are theoretical results from Ref. 13. The electric field $F$ (upper scale) is calculated according to Eq. (10).

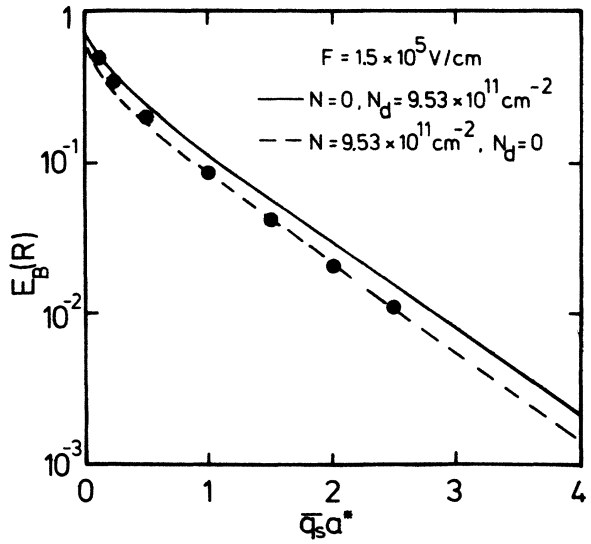


FIG. 14. Binding energy versus screening parameter according to the separable potential approximation and the modified Thomas-Fermi approximation as full and dashed lines for the electric field $F = 1.5 \times 10^5$ V/cm. The dots according to Ref. 12 for the same electric field.

too small for $N=0$. We mention that in this case the binding energy for finite electron density is determined by the electron density. The ideally two-dimensional electron gas with $E_B=4R$ is outside the range of the experimental possibility.

We can also calculate the binding energy for a screened potential in the limit $N_i \to 0$. The screening reduces the binding energy drastically. For $N_d=3.6\times10^{11}$ cm$^{-2}$ and $N=1\times10^{13}$ cm$^{-2}$ within the RPA we get a binding energy $E_B=(4\times10^{-3})R$. In the Klauder approximation we find for the same parameters $E_B=(6\times10^{-3})R$, while Vinter[13] gets $(1.4\times10^{-2})R$ using the density-functional theory. The binding energy depends in a sensitive way on the screening function. For high electron densities the bound states become very shallow.

In Fig. 14 we have shown our results on the binding energy versus the screening parameter. We used the separable potential approximation and the modified Thomas-Fermi approximation in the following form: $\epsilon(q)=1+F_c(q)\bar{q}_s/q$. According to Eq. (10), various sets of $N$ and $N_d$ result in an electric field $F=1.5\times10^5$ V/cm, which was used in the single-impurity approach of Ref. 12. The two sets of $N$ and $N_d$ which we used in Fig. 14 are in reasonable agreement with Ref. 12.

## VII. DISCUSSION AND COMPARISON WITH EXPERIMENTS

In this section we compare our theoretical results on the DOS with experimental results found in sodium-doped silicon MOSFET systems.

### A. Conductivity measurements in the impurity band

In the conductivity versus electron-density measurements on sodium-doped silicon inversion layers[2-4] the following behavior has been discovered: For lower sodium concentrations (typically $5\times10^{11}$ cm$^{-2}$) a peak in the conductivity at low electron density (typically $1\times10^{11}$ cm$^{-2}$) is found.[4] For higher electron densities the conductivity increases rapidly with increasing $N$. The peak was interpreted as an IB induced by the sodium ions, and the strong increase of the conductivity at higher electron densities was interpreted as the conduction in the CB. For higher impurity concentrations (typically $1\times10^{12}$ cm$^{-2}$) the peak in the conductivity disappears. This behavior was interpreted as a merging of the IB with the CB (band-tail description).

We agree with this interpretation. Our theoretical results (see Fig. 1 and the insets of Figs. 4 and 11) are in qualitative agreement with the experimental results. For low impurity concentrations we found an IB, while a BT occurs for higher impurity concentrations.

Quantitatively our impurity concentration $\tilde{N}_i$, where the IB merges with the CB, is reduced by a factor of 10 compared to experiments. For $N_d=3\times10^{11}$ cm$^{-2}$ and $N=2\times10^{11}$ cm$^{-2}$ $(1\times10^{11}$ cm$^{-2})$ we found $\tilde{N}_i=0.5\times10^{11}$ cm$^{-2}$ $(1\times10^{11}$ cm$^{-2})$ [compare with Fig. 1 (Fig. 4)]. Our electron density, for which the IB is filled using $g_sg_v=1$ (see inset of Fig. 4), compares well with the experimental results.[4] Of the first experimental measurements it was claimed[38] that there is one electron state for each oxide charge in the IB. This implies that the spin and valley degeneracies are lifted [see Eq. (19)]. Recent experimental results,[4] however, show the following behavior: For $N_i=3.4\times10^{11}$ cm$^{-2}$ and $N_i=9.3\times10^{11}$ cm$^{-2}$ the electron densities necessary to fill up the IB are found to be $1\times10^{11}$ cm$^{-2}$ and $3\times10^{11}$ cm$^{-2}$, respectively. We conclude that the effective impurity concentration which contributes to the IB is 3 times smaller for $g_sg_v=1$ and 12 times smaller for $g_sg_v=4$ than the experimentally determined impurity density. The factor of 3 has also been used in Ref. 4 to describe the temperature dependence of the conductivity within the model for hopping conduction[39] in the IB, where the DOS of the IB is the input. The misfit, found experimentally between $N$ and $N_i$, will be discussed below. With the factor of 3 the impurity concentration turns into a typical $3\times10^{11}$ cm$^{-2}$, where the peak in the conductivity disappears.[4] In comparison to our theoretical result $\tilde{N}_i=1\times10^{11}$ cm$^{-2}$ (see the inset in Fig. 4), a discrepancy of a factor of 3 remains.

For the discussion of the hopping conduction it was assumed in Ref. 4 that the DOS in the IB is constant and given by $N_i/W$ and that $W$ is the width of the IB. In order for the theory and the experiment to agree well, a decrease of $W$ from 10 meV at $N_i=3\times10^{11}$ cm$^{-2}$ to 3 meV at $N_i=12\times10^{11}$ cm$^{-2}$ was found to be necessary. The unexplained behavior of the decreasing width with increasing impurity density raises the question whether the assumptions on the hopping conduction model are realistic. In our theory the width increases with increasing impurity concentration and is of the size of the binding energy.

In the separable potential approximation with an unscreened potential (see Fig. 10) our theoretical value $\tilde{N}_i=5\times10^{11}$ cm$^{-2}$ is in better agreement with the experimental results. However, the electron density scale in Fig. 11 is two times too large (for $g_sg_v=1$) in comparison to the experiments.[4] Since we only have a mathematical but no physical motivation to use the separable potential, we do not believe as much in figures which result from the separable potential approximation.

The depletion density was varied in Ref. 4 by a substrate bias. It was found that for fixed $N_i$ the maximum of the conductivity in the IB decreases with decreasing $N_d$. This is in qualitative agreement with our results; see Fig. 3.

Conductivity versus electron-density measurements have also been taken on sodium-doped accumulation layers.[40] The peak structure which was found in the dynamical conductivity was quantitatively attributed to plasmon dynamics.[41] No indications for an IB in accumulation layers have been seen in experiments for $N_i>2\times10^{11}$ cm$^{-2}$, which is nearly the residual impurity density of the studied accumulation layers.[42] This is in qualitative agreement with our results (see Fig. 3 for $N_d=0$). The binding energy is decreasing with decreasing $N_d$ (see Fig. 13). It is obvious that $\tilde{N}_i$ also decreases with decreasing $N_d$.

In our model we have assumed that all impurities are located at the interface of the oxide and the semiconductor. In experiments it was found that the sodium ions are

located within 50 Å of the interface.[43] Different distributions of the sodium within this distance might be realized in different samples. A discussion on the difficulties to determine the impurity density in experiment can be found in Refs. 44 and 45. We have found that $\tilde{N}_i(z_i)$ decreases if the impurities are moved from the interface to the oxide. For given $N_i > \tilde{N}_i(z_i)$ for $z_i > 0$ the remote impurities result in a BT in the DOS, but for the same $N_i < \tilde{N}_i(z_i = 0)$ the impurities at the interface result in an IB. This might be the reason why an effective impurity concentration has to be introduced in the experiment of Ref. 4.

The Klauder approximation for a distribution of impurities in the oxide is discussed in the Appendix. We mention, however, that the mobility versus electron-density measurements, where the Fermi energy is in the CB, have been quantitatively explained theoretically[46] by assuming the impurities to be located at the interface and by using the experimental values $N_i$.[47]

### B. Deep-level transient spectroscopy (DLTS) measurements

DLTS measurements have been performed with sodium drifted silicon MOSFET systems. In the recent experiment[5] the DOS versus sodium concentration was determined in the band gap for $E = -1.8R$. A strong increase of the DOS for $N_i \geq 3\times 10^{12}$ cm$^{-2}$ was found.

In Fig. 15 we show the DOS versus energy for $N = 1\times 10^{11}$ cm$^{-2}$, $N_d = 3\times 10^{11}$ cm$^{-2}$ and high impurity density ($1\times 10^{12}$ cm$^{-2} < N_i < 1\times 10^{13}$ cm$^{-2}$). We used the Klauder approximation and the RPA. With increasing impurity density the CB edge shifts to lower energy. The shift $\Delta E_{e\text{-}i}$, due only to the disorder, is given by

$$\Delta E_{e\text{-}i} = -0.88R \left[ \frac{N_i}{10^{12}\ \text{cm}^{-2}} \right]^{0.46} . \tag{31}$$

In the separable potential approximation we find within the RPA

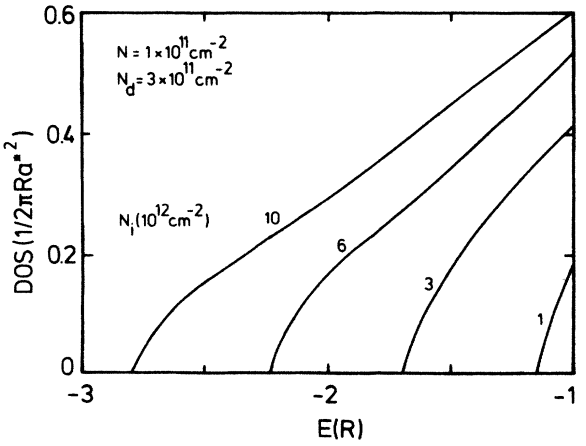


FIG. 15. Density of states versus energy for high impurity concentrations according to the Klauder approximation and the random-phase approximation.

$$\Delta E_{e\text{-}i} = -0.64R \left[ \frac{N_i}{10^{12}\ \text{cm}^{-2}} \right]^{0.49} . \tag{32}$$

From Fig. 15 it becomes obvious that for a given energy a threshold impurity density $\bar{N}_i$ exists, below which $\rho(E)=0$, while for $N_i > \bar{N}_i$ the DOS increases with $N_i$. From Fig. 15 we find $\bar{N}_i = 4\times 10^{12}$ cm$^{-2}$ for $E = -1.8R$. The DOS for this energy and for $N_i > \bar{N}_i$ is ten times larger than in experiment[5] (for $g_s g_v = 1$). This might be due to a distribution of impurities into the bulk of the oxide, as discussed before. In addition we expect impurity concentration fluctuation effects to be important at the CB edge.[17,19]

Similar results have been found within the unscreened separable potential approximation. However, there is no sharp increase of the DOS for a certain threshold impurity density because the unscreened potential has a very long low-energy BT.

### C. Infrared measurements

Far-infrared measurements of the intersubband absorption in sodium-drifted silicon MOSFET systems have been reported.[48,49]

The experiments on inversion layers[48] with $N_d = 1\times 10^{11}$ cm$^{-2}$ showed a positive sodium induced shift of the resonance for fixed electron density. This shift was saturated for $N_i > 4\times 10^{11}$ cm$^{-2}$. For fixed sodium concentration the disorder induced shift seems to disappear for $N > 2N_i$. The resonance for $N < 2N_i$ has been interpreted as a transition from an IB associated with the zeroth subband to an IB associated with the first subband. The disappearance of the shift for $N > 2N_i$ has been interpreted as a screening effect.[48] Yet it is unclear to us which structures of the DOS can be seen in the intersubband absorption measurements. Our theory gives some indication why the split-off IB disappears for fixed $N_d$ and $N_i$ and a BT appears when the electron density increases. This effect is attributable to screening. In Fig. 4 the DOS versus energy for $N_i = 1\times 10^{11}$ cm$^{-2}$ is shown. For $N < 1\times 10^{11}$ cm$^{-2}$ we found an IB and for $N > 2\times 10^{11}$ cm$^{-2}$ a BT.

The saturation of the sodium-induced shift was not explained in Ref. 48. Within a BT situation we would expect that for high $N_i$ a transition from the zeroth subband to the edge of the first subband depends on $N_i$ only weakly. The impurities have a stronger effect on the zeroth subband than on the first subband because the latter is more extended into the bulk. The $N_i$ dependence of the edge of the zeroth subband is a weak one for the studied impurity density according to Eq. (31).

The experiments on accumulation layers[49] also exhibit a positive sodium-induced shift of the resonance. Because of the absence of IB's in accumulation layers and the increase of the shift with increasing $N_i$, the effect has been explained as a plasmon effect.[49]

## VIII. CONCLUSION

We have used a multiple scattering method to calculate the electronic structure of a two-dimensional electron

gas, i.e., the inversion and the accumulation layers in sodium-doped silicon MOSFET systems.

Within a separable potential approximation the simplified Klauder's equations have been discussed and the results have been compared with those obtained from the complete solution; see also Ref. 50.

We have shown how the band tail is transformed into a split-off impurity band below a certain impurity concentration. This concentration is found to vary with electron and depletion densities.

Our description of electronic properties of these two-dimensional systems are in qualitative agreement with recent experiments on impurity band conductivity[4] and infrared absorption,[48] in sodium-doped silicon MOSFET systems as well as with deep band tails found in deep-level transient spectroscopy.[5] A good quantitative agreement between our theory and the experiment could be reached if it is assumed that a fraction of impurities lies inside the bulk, instead of at the interface.

## ACKNOWLEDGMENTS

We thank F. Koch for critical and encouraging discussions. A. Gold was supported by the Ernst von Siemens Siftung of the Siemens Aktiengesellschaft. The Groupe de Physique des Solides de l'Ecole Normale Supérieure is a "Laboratoire associé au Centre National de la Recherche Scientifique."

## APPENDIX: THE GENERALIZED KLAUDER EQUATIONS

The Klauder equation [see Eq. (6)] has to be generalized for different kinds of scatterers. For a two-dimensional impurity sheet in the oxide at a distance $z_i$ from the interface the electron-impurity interaction potential is given by

$$V_{e\text{-}i}(\mathbf{q},z_i)=\frac{2\pi Ze^2}{\epsilon_L}\frac{1}{q}\frac{1}{(1+q/b)^3}e^{-qz_i} . \tag{A1}$$

The screened potential is expressed as

$$V(\mathbf{q},z_i)=\frac{V_{e\text{-}i}(\mathbf{q},z_i)}{\epsilon(\mathbf{q})} . \tag{A2}$$

The generalized (fifth) Klauder's approximation for $M$ sheets of impurities is rewritten for $i=1,\ldots,M$ as

$$K(\mathbf{k},\mathbf{q},E,z_i)=N_i(z_i)V(\mathbf{q}-\mathbf{k},z_i)+\frac{1}{(2\pi)^2}\int d^2q'V(\mathbf{q}-\mathbf{q}',z_i)\times G(\mathbf{q}',E)U(\mathbf{k},\mathbf{q}',E,z_i) . \tag{A3}$$

$N_i(z_i)$ is the two-dimensional impurity density in the sheet at $z_i$. The quantity

$$\Sigma(\mathbf{k},E,z_i)=U(\mathbf{k},\mathbf{k},E,z_i)-N_i(z_i)V(0,z_i) \tag{A4}$$

determines the self-energy

$$\Sigma_{e\text{-}i}(\mathbf{k},E)=\sum_{i=1}^{M}\Sigma(\mathbf{k},E,z_i) , \tag{A5}$$

$$\Sigma(\mathbf{k},E)=\Sigma_{e\text{-}i}(\mathbf{k},E)+\Sigma_{xc}(\mathbf{k},E) \tag{A6}$$

and the Green function is expressed as

$$G(\mathbf{k},E)=\frac{1}{E-\varepsilon(\mathbf{k})-\Sigma(\mathbf{k},E)} . \tag{A7}$$

By increasing the number of impurity sheets the set of integral equations (A1)–(A7), however, becomes difficult to solve.

In the separable potential approximation we find

$$\Sigma_{e\text{-}i}(\mathbf{k},E)=Z^2C(2)\sum_{i=1}^{n}N_i(z_i)\frac{V(k,z_i)B(E,z_i)}{1-ZB(E,z_i)} \tag{A8}$$

and

$$B(E,z_i)=\frac{C(2)}{2\pi}\int_0^\infty dq\, qV(q,z_i)G(q,E) \tag{A9}$$

for $d=2$. In the limit $N_i(z_i)\to 0$ we express the condition for bound states as

$$1-ZB^0(E,z_i)=0 \tag{A10}$$

for $i=1,\ldots,M$ with

$$B^0(E,z_i)=\frac{C(2)}{2\pi}\int_0^\infty dq\, qV(q,z_i)\frac{1}{E-\varepsilon(\mathbf{q})} . \tag{A11}$$

It is obvious that our model has the property to explain qualitatively the $N$ and $N_i$ misfit in the conductivity measurement in IB's found in the experiment.[4] The generalized Klauder's equations are also relevant for the band gap renormalization and for homogeneously distributed background impurities. This will be discussed elsewhere.

*Present address: Physik Department E16, Technische Universität München, D-8046 Garching, Federal Republic of Germany.

[1]T. Ando, A. B. Fowler, and F. Stern, Rev. Mod. Phys. **54**, 437 (1982).
[2]A. Hartstein and A. B. Fowler, Phys. Rev. Lett. **34**, 1435 (1975); Surf. Sci. **73**, 19 (1978).
[3]A. B. Fowler and A. Hartstein, Philos. Mag. B **42**, 949 (1980).
[4]G. Timp, A. B. Fowler, A. Hartstein, and P. N. Butcher, Phys. Rev. B **34**, 8771 (1986).
[5]E. Rosencher and R. Copard, J. Appl. Phys. **55**, 971 (1984), and references cited therein.
[6]J. D. Levine, Phys. Rev. **140**, A586 (1965).
[7]F. Stern and W. Howard, Phys. Rev. **163**, 816 (1967).
[8]A. V. Chaplik and M. V. Entin, Zh. Eksp. Teor. Fiz. **61**, 2496 (1971) [Sov. Phys.—JETP **34**, 1335 (1972)].
[9]N. O. Lipari, J. Vac. Sci. Technol. **15**, 1412 (1978).
[10]B. G. Martin and R. F. Wallis, Phys. Rev. B **18**, 5644 (1978).
[11]B. Vinter, Solid State Commun. **28**, 861 (1978).
[12]O. Hipolito and V. B. Campos, Phys. Rev. B **19**, 3083 (1979).

[13]B. Vinter, Phys. Rev. B **26**, 6808 (1982).
[14]I. C. da Cunha Lima, A. Ferreira da Silva, P. S. Guimarães, L. F. Perondi, and J. R. Senna, Phys. Rev. B **32**, 2371 (1985); E. A. de Andrada e Silva and I. C. da Cunha Lima, Phys. Rev. Lett. **58**, 925 (1987).
[15]Y. Ishida and F. Yonezawa, Prog. Theor. Phys. **49**, 731 (1973).
[16]M. Takeshima, Phys. Rev. B **33**, 4045 (1986); **34**, 1041 (1986).
[17]B. I. Halperin and M. Lax, Phys. Rev. **148**, 722 (1966).
[18]U. Ekenberg, Phys. Rev. B **30**, 3367 (1984).
[19]J. Serre, A. Ghazali, and P. Leroux Hugon, Phys. Rev. B **23**, 1971 (1981).
[20]P. A. Lee and T. V. Ramakrishnan, Rev. Mod. Phys. **57**, 287 (1985).
[21]E. P. Abrahams, P. W. Anderson, D. C. Licciardello, and T. V. Ramakrishnan, Phys. Rev. Lett. **42**, 673 (1979); G. Bergmann, Phys. Rep. **101**, 1 (1984).
[22]F. Wegner, Z. Phys. B **44**, 9 (1981).
[23]W. Götze, Philos. Mag. B **43**, 219 (1981); A. Gold and W. Götze, J. Phys. C **14**, 4049 (1981).
[24]L. Efros and B. I. Shklovskii, J. Phys. C **8**, L49 (1974).
[25]M. Pollak, Discuss. Faraday Soc. **50**, 13 (1970); M. Pollak and M. L. Knotek, J. Non-Cryst. Solids **32**, 141 (1979).
[26]B. L. Altshuler, A. G. Aronov, and P. A. Lee, Phys. Rev. Lett. **44**, 1288 (1980).
[27]J. R. Klauder, Ann. Phys. (N.Y.) **14**, 43 (1961).
[28]A. Ghazali and J. Serre, Phys. Rev. Lett. **48**, 886 (1982); J. Serre and A. Ghazali, Phys. Rev. B **28**, 4704 (1983).
[29]R. Schwabe, A. Haufe, V. Gottschalch, and K. Unger, Solid State Commun. **58**, 485 (1986).
[30]A. Abrikosov, L. Gorkov, and I. Dzyaloshinskii, *Quantum Field Theoretical Methods in Statistical Physics* (Pergamon, Oxford, 1965).
[31]T. Ando, A. B. Fowler, and F. Stern, Rev. Mod. Phys. **54**, 619 (1982).
[32]D. Pines and Ph. Nozieres, *The Theory of Quantum Liquids* (Benjamin, New York, 1966).
[33]J. Alvarellos and F. Flores, J. Phys. F **15**, 2465 (1985).
[34]B. Vinter, Phys. Rev. B **13**, 4447 (1976).
[35]P. Leroux Hugon and A. Ghazali, Phys. Rev. B **14**, 602 (1976).
[36]A. Gold, Phys. Rev. A **33**, 652 (1986).
[37]H. Ehrenreich and L. M. Schwartz, in *Solid State Physics*, edited by F. Seitz, D. Turnbull, and H. Ehrenreich (Academic, New York, 1976), Vol. 31, Sec. IV 13, p. 149.
[38]A. Hartstein and A. B. Fowler, in *Proceedings of the 13th International Conference on the Physics of Semiconductors, Rome, 1976*, edited by F. G. Fumi (North-Holland, Amsterdam, 1976), p. 741.
[39]K. Hayden and P. Butcher, Philos. Mag. B **38**, 603 (1979).
[40]H. R. Chang and F. Koch, Surf. Sci. **113**, 114 (1982).
[41]A. Gold, W. Götze, C. Mazure, and F. Koch, Solid State Commun. **49**, 1085 (1984).
[42]C. Mazure, Ph.D. dissertation, Technische Universität München, 1985.
[43]D. J. Di Maria, J. Appl. Phys. **48**, 5149 (1978).
[44]A. B. Fowler and A. Hartstein, Surf. Sci. **98**, 169 (1980).
[45]J. E. Furneaux and T. L. Reinecke, Phys. Rev. B **33**, 6897 (1986).
[46]A. Gold, Phys. Rev. B **32**, 4014 (1985); Phys. Rev. Lett. **54**, 1079 (1985).
[47]A. Gold, Surf. Sci. **170**, 381 (1986).
[48]E. Glaser, R. Czaputa, B. D. Mc.Combe, G. M. Kramer, and R. F. Wallis, Phys. Rev. Lett. **57**, 893 (1986).
[49]C. Mazure, F. Martelli, A. Gold, U. Grzesik, H. R. Chang, and F. Koch, Solid State Commun. **54**, 443 (1985).
[50]A. Ghazali, A. Gold, and J. Serre, Proceedings of the VIIth Conference on the Electronic Properties of Two-Dimensional Systems, Santa Fe, 1987 [Surf. Sci. (to be published)].